International Journal of Design & Nature and Ecodynamics
Vol. 21, No. 1, January, 2026, pp. 129-137
Journal homepage: http://iieta.org/journals/ijdne

Solar-Light-Driven Photodegradation of Paracetamol Using Green-Synthesized TiO_2 Nanoparticles from *Eucalyptus globulus* Leaf Extract

Rasha Waleed Al-Khateeb[1*], Raghad N. Mohammed[2], Abeer I. Alwared[2], Noor A. Mohammed[2]

[1] Department of Physics, University of Baghdad, Baghdad 10071, Iraq
[2] Department of Environmental Engineering, University of Baghdad, Baghdad 10071, Iraq

Corresponding Author Email: Rasha.w@sc.uobaghdad.edu.iq

https://doi.org/10.18280/ijdne.210112

Received: 8 November 2025
Revised: 15 January 2026
Accepted: 23 January 2026
Available online: 31 January 2026

Keywords:
green synthesis, eucalyptus leaf, TiO_2, paracetamol, solar light

ABSTRACT

In this study, *Eucalyptus globulus* leaf extract was utilized to fabricate TiO_2 nanoparticles (denoted as E-TiO_2) by using a green synthesis method. X-ray Diffraction (XRD), Fourier Transform Infrared Spectroscopy (FTIR), and Scanning Electron Microscopy (SEM) techniques were used to confirm the formation, particle size, and shape of the synthesized E-TiO_2 particles. In the presence of sunlight, the efficacy of E-TiO_2 nanoparticles was examined for their photocatalytic decomposition of paracetamol (PC) residues from aqueous solutions at different operating conditions, including pH (3, 5, 7, and 11), initial PC dosage (10, 25, and 100) mg/L, E-TiO_2 dosage (20, 40, and 100) mg/L, concentration of H_2O_2 (150, 250, 400, and 600) mg/L. At the best operating conditions of pH 7, E-TiO_2 dosage 40 mg/L, PC dosage 10 mg/L, and H_2O_2 concentration 250 mg/L, respectively, the proposed E-TiO_2 demonstrated high efficiency in the treatment of PC contaminated water 94.13% while commercial TiO_2 achieved only 78.23% at the same degradation time (120 min). Additionally, a first-order kinetics model with $R^2 > 98\%$ was followed by the reaction. The findings demonstrated that E-TiO_2 nanocomposite exhibits commendable efficiency in the degradation of PC, with its relatively straightforward synthesis rendering it an appropriate nanoparticle for the removal of pharmaceutical residues, alongside remarkable reusability and stability, evidenced by the negligible loss in photocatalytic activity over multiple cycles.

1. INTRODUCTION

Pharmaceuticals are extensively used in fishing, medicine, animal husbandry, and other areas, which has resulted in their constant presence in the environment and possible threats to human health and the ecology. A proportion ranging from approximately 11% to 85% of pharmaceutical compounds is excreted without undergoing metabolic transformation. Even though pharmaceutical chemicals are only found in small amounts in home wastewater, they are mostly between ng L^{-1} to µg L^{-1}, their chemically stable and physiologically resistant characteristics make their total removal from wastewater treatment systems difficult [1, 2]. The issue is made worse by the COVID-19 pandemic, which the World Health Organization states has caused 5 million deaths and nearly 250 million confirmed cases. Despite the widespread use of medications, especially for symptom relief, controlling COVID-19 remains a significant global issue. Paracetamol (PC) (4-hydroxyacetanilide, 4-acetamidephenol, acetaminophen, or Tylenol) is one such drug used to lower fever and ease COVID-19-related muscle soreness. However, the extensive usage of drugs like acetaminophen contaminates the environment and jeopardizes the biosphere [3, 4]. PC was detected in wastewater treatment facility effluents at amounts as high as 6 µg/L. Due to the growing population and their modern lifestyles, paracetamol concentrations in water and wastewater may increase. The manufacturing of paracetamol has expanded dramatically worldwide as a result of the sharp rise in usage [5]. Different treatment technologies are improved for the elimination of pharmaceuticals, encompassing photocatalysis, electrochemical treatment processes, adsorption, membrane filtration, biological treatment, and disinfection, which is under investigation [6]. However, biological treatment methods often take longer than chemical ones and are ineffective for very persistent pollutants [7, 8]. Thus, due to their high operational cost and low removal efficiency, they are not widely applied. Therefore, Antibiotics' capacity to inhibit bacteria has been improved by the use of advanced oxidation processes (AOPs), which also increased the biodegradability and elimination rate of the antibiotics [9]. In general, advanced oxidation processes (AOPs) degrade pollutants by generating highly reactive species, such as hydroxyl radicals (•OH), sulfate radical (SO_4), and superoxide radical ($O_2^{\bullet-}$), which react with pollutants at near diffusion-controlled rates [10]. Among various AOPs, photocatalytic degradation of toxicants has become one of the most promising approaches in green chemistry [11]. Among the many types of catalysts, TiO_2 NPs have been used because it has a high surface area, uniform pore size, and highly reactive surface atoms. In aqueous photocatalytic systems, TiO_2

nanoparticles function as catalyst supports. The interaction of water molecules adsorbed on their surfaces significantly affects the surface reaction pathways [12]. The nanoparticles biosynthesis is a green synthetic process, which involves employing reducing agents, that are biologically sourced, i.e. plants and microorganisms. Such an approach is characterized by various important merits such as the safety of the environment, low cost, biocompatibility, renewability, and non-toxicity [13]. To this end, numerous scholars have utilized diverse plant extracts, such as leaves of *Zizyphus spina-christi* [14], a blend of extracts of *Piper betel*, *Ocimum tenuiflorum*, *Moringa oleifera*, and *Coriandrum sativum* to synthesize nano-TiO_2 [15], and grape leaves [16]. The conversion of bio-based waste into valuable products offers substantial potential for advancing global economic development while simultaneously addressing waste management challenges [17, 18]. There are various benefits of using plant extracts to create nanomaterials: (i) Plant material is easily accessible; (ii) Operational safety; (iii) Minimal running expenses; (iv) The biomolecules present in the extracts' capacity to function as stabilizing, capping, and reducing agents; (v) Removing complex bacterial, fungal, and yeast maintenance; (vi) Quick synthesis methods; (vii) Using eco-friendly procedures; (viii) Creating nanoparticles that are more stable; (ix) The potential for improved control over the nanoparticles' size and shape; (x) Large-scale suitability [19]. Eucalyptus trees are quite widespread throughout China, which can be explained by their high viability, low cost of cultivation, and the abundance of polyphenolic compounds; the utilization of the material of the eucalyptus leaves produces a significant environmental impact with the reduction of waste and the creation of added value when preparing titanium nanoparticles [20]. Many previous studies utilized eucalyptus leaf extract for the synthesis of TiO_2 nanoparticles, such as Balaji et al. [12] employed the resulting TiO_2 as a catalyst in one-pot, three-component A3 coupling reactions; Torres-Limiñana et al. [21] used them in bacteria inhibition; Uwaya et al. [22] assessed the interaction between efavirenz and TiO_2 NPs employed as an analytical nano-vehicle. Our study is concerned with the synthesis of TiO_2 NPs prepared from the eucalyptus leaf extract, and testing the ability to degrade PC from aqueous solution by a heterogeneous photocatalyst, investigating the characteristics of the TiO_2 NPs via Fourier Transform Infrared Spectroscopy (FTIR), X-ray Diffraction (XRD), Scanning Electron Microscopy (SEM), and Brunauer–Emmett–Teller Surface Area Analysis (BET), and evaluating the PC elimination percentage under various experimental conditions.

2. MATERIALS AND METHODS

2.1 Materials

The chemical materials used in this study are: powdered paracetamol (PC, 99%), and their chemical structures and specifications are provided in Figure 1 and Table 1, respectively. The precursor, Titanium Tetra-Isopropoxide (TTIP), consisted of 95% anatase and 5% rutile phases. Isopropanol and hydrogen peroxide (H_2O_2, 50 w/w%). These materials, requiring no further purification, were obtained from Merck. The pH of the aqueous solutions was adjusted to the desired values using hydrochloric acid or sodium hydroxide.

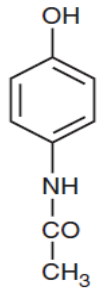

Figure 1. Paracetamol chemical structure [23]

Table 1. Main properties of paracetamol [24]

Parameters	Character/Value
Molecular formula	$C_8H_9NO_2$
Molar mass	151.163 g/mol
Water solubility at 25°C (g/L)	13.85
Dissociation constant (pKa)	9.4

2.2 Methods

2.2.1 Leaves extract preparation

Fresh leaves were collected from eucalyptus trees located in Baghdad, Iraq, first washed twice or thrice with tap water then distilled water and dried at ambient temperature during a week in a chamber devoid of dust in a parallel protocol, powdered and 10 g of the fine powder was put in boiling water of 100 mL and left to extract after 15 min to get an aqueous extract. The aqueous extract was filtered, centrifuged at 5000 rpm, and the supernatant was refrigerated at 4°C to prevent contamination by microbes [12].

2.2.2 Green synthesis of E-TiO_2 NPs

E-TiO_2 NPs were prepared by dropwise adding 50 mL of eucalyptus leaves extract to a solution of (3 mL of TTIP + 50 mL of ethanol), which was added dropwise in the ratio of 1:1 (v/v). The mixture was stirred constantly for two to three hours until a brownish-yellow precipitate formed, then after the mixture was centrifuged at 10,000 rpm for 15 min and cleaned with ethanol twice times in order to get rid of any remaining contaminants. The brownish-yellow precipitate was thoroughly pulverized with an agate mortar and pestle, dried for 2 hours at 80°C in a hot air oven, and then calcinated at 500°C for 3 hours [12].

2.2.3 Procedure and analysis

Batch solar photocatalytic decomposition experiments were performed in a Pyrex mode reactor under natural sunlight (Figure 2). A mirror positioned at the bottom of the Pyrex enhanced irradiation by reflecting additional solar light onto the reaction mixture. On successive sunny days in June and July of 2025, the solutions were exposed to direct solar radiation from 12 a.m. to 3 p.m. SPM-1116SD was used to measure the amount of solar radiation that reached the reactor. Batch solar photocatalytic decomposition experiments were performed in a Pyrex mode reactor under natural sunlight (Figure 2). A mirror positioned at the bottom of the Pyrex enhanced irradiation by reflecting additional solar light onto the reaction mixture. On successive sunny days in June and July of 2025, the solutions were exposed to direct solar radiation from 12 a.m. to 3 p.m. SPM-1116SD was used to measure the amount of solar radiation that reached the reactor.

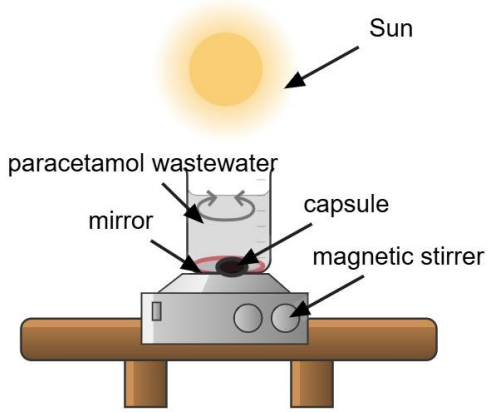

Figure 2. Schematic of the solar photo-oxidation process

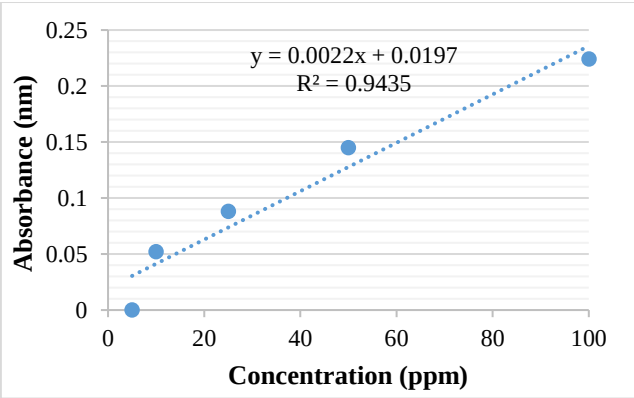

Figure 3. Standard curve of paracetamol

PC solutions with concentrations of 10, 25, and 100 g/L were prepared, and the pH was adjusted using 1 M HCl or NaOH. E-TiO_2 nanoparticles were added at concentrations of 20, 40, or 100 mg/L. The suspensions were magnetically stirred (MSH-300N, BOECO, Hamburg, Germany) at 200 rpm for 120 minutes. An initial dark period of 30 minutes allowed adsorption equilibrium between PC and the E-TiO_2 surface. Subsequently, H_2O_2 (150, 250, 400, or 600 mg/L) was introduced, and the reaction mixture was exposed to sunlight to initiate photocatalysis. Aliquots of 10 mL were collected at predetermined intervals. The catalyst was separated by centrifugation at 2000-5000 rpm for 15 minutes, and the supernatants were analyzed using a Perkin–Elmer 55 OSE UV–Vis spectrophotometer at 243 nm, where the standard curve was examined at 5, 10, 25, 50, 100, and 150 mg/L, as indicated in Figure 3. The degradation percentage efficiency of PC was determined by using Eq. (1):

$$PC\ elimination\ percentage = \frac{C_o - C_e}{C_o} \times 100 \qquad (1)$$

where, C_o and C_e are the initial and final concentrations of PC (mg/L), respectively.

3. RESULTS AND DISCUSSION

3.1 E-TiO_2 NPs characterization

3.1.1 X-ray Diffraction analysis

The crystalline structure of the synthesized metallic nanoparticles was investigated using XRD, following the methodology of Huang et al. [25]. E-TiO_2 nanoparticles were examined with a SMART Bruker D8 Advance diffractometer using Cu Kα radiation (λ = 1.54 Å). Diffraction patterns were recorded over a 2θ range of 10–80° to assess both the phase composition and crystallinity of the nanoparticles. The obtained diffraction pattern was compared with the standard JCPDS file No. 21-1272 [12], which confirmed that the indexed hkl reflections—25° (101), 38° (112), 48° (200), 55° (211), and 63° (204)—correspond to the anatase polymorph. As illustrated in Figure 4, the E-TiO_2 nanoparticles exhibit a tetragonal crystal lattice. The average crystal size for E-TiO_2 was 40.123nm, while that for commercial TiO_2 was 25 nm, determined using Scherrer's equation (Eq. (2)).

$$D = \frac{K\lambda}{\beta cos\theta} \qquad (2)$$

where, D is crystallite size, β is the full width at half maximum (FWHM) of diffraction peak to the corresponding crystallographic plane of anatase, θ is the angle of the X-ray Diffraction peak, K represents Scherrer constant (0.94), λ is defined as a wavelength of X-ray radiation (0.15418 Å) [14].

3.1.2 Scanning and electron microscopy

The adsorbent's surface morphology before and after the adsorption was examined using SEM analysis. Figure 5(a) illustrates the SEM image of the E-TiO_2 NPs before treatment, while Figure 5(b) represents the surface morphology after the degradation of the PC. And the findings of Figure 5(a) demonstrated the morphology of the E- TiO_2 before treatment with a relatively uniform, but irregular, surface, characterized by spherical irregular aggregates [26]. The availability of microscopic pores and numerous cavities was also a further sign of the suitability of E-TiO_2 NPs to be used in photocatalytic applications [27]. Figure 5(b) shows that the morphological changes on E-TiO_2 that occurred during PC adsorption were pronounced. When the pore surfaces became filled with the antibiotic particles, it was possible to observe changes in the catalyst surface, which became less rough and smoother, and some formerly separated aggregates became mixed. The main factor, which might have led to the high antibiotic uptake, is possibly the obvious pores of the catalyst, since adsorption is performed on the active surface groups present on the pore.

3.1.3 Fourier Transform Infrared Spectroscopy analysis

FTIR analysis is a powerful method for identifying functional groups present on nanoparticle surfaces; thus, it was employed to characterize the E-TiO_2 samples before (black spectrum) and after (red spectrum) use in removing PC from aqueous solutions. As illustrated in Figure 6 (black spectrum), the absorption bands appearing between 500 and 800 cm^{-1} correspond to Ti–O stretching vibrations, confirming the formation of TiO_2 nanoparticles. The band at 2843.52 cm^{-1} is assigned to C–H stretching of aldehyde groups, whereas the peak at 1643.61 cm^{-1} arises from the H–O–H bending vibration of adsorbed water and/or the C=O stretching vibration of residual organic species originating from the plant extract used during synthesis, accompanied by CH_3 stretching at 2921.63 cm^{-1}. In addition, the broad absorption associated with –OH stretching and bending appears at 3423.99 cm^{-1}, and the Ti–O–Ti stretching mode is detected at 1395.28 cm^{-1} [15]. Following PC degradation (red spectrum in Figure 6), noticeable changes in peak intensities were observed, indicating adsorption or chemical interaction between the

active surface groups of the catalyst and PC molecules or adsorption [28, 29].

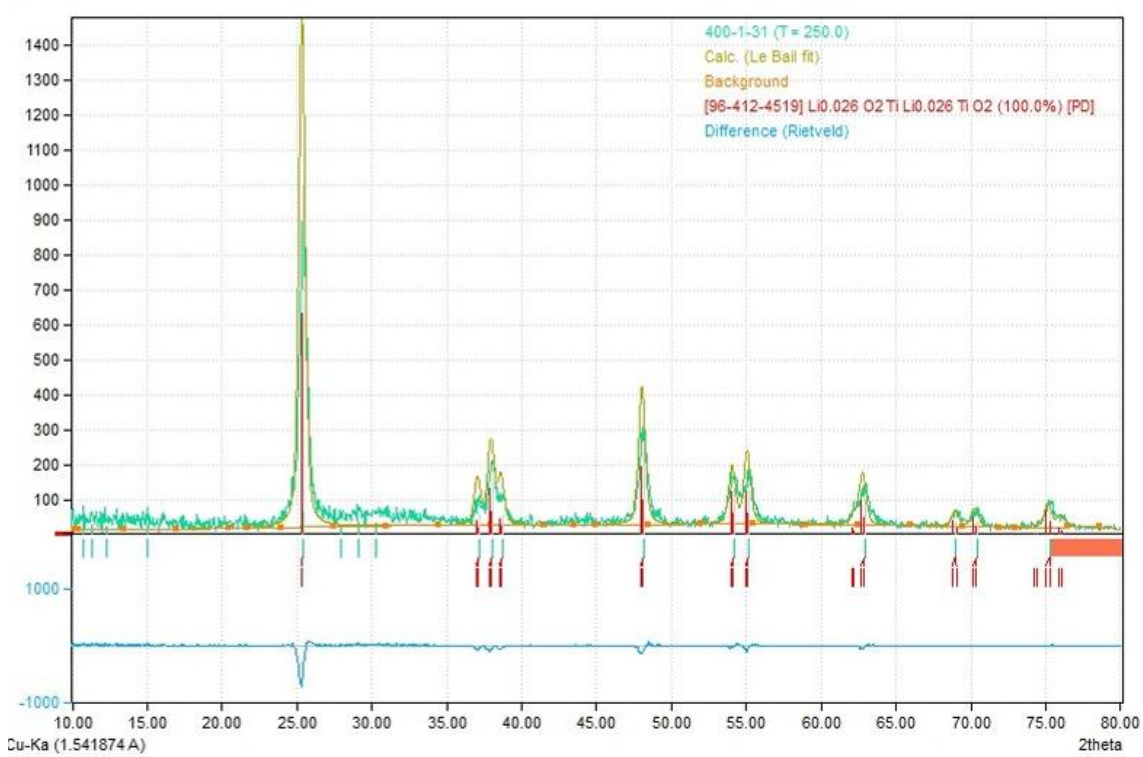

Figure 4. X-ray Diffraction (XRD) pattern for E-TiO_2

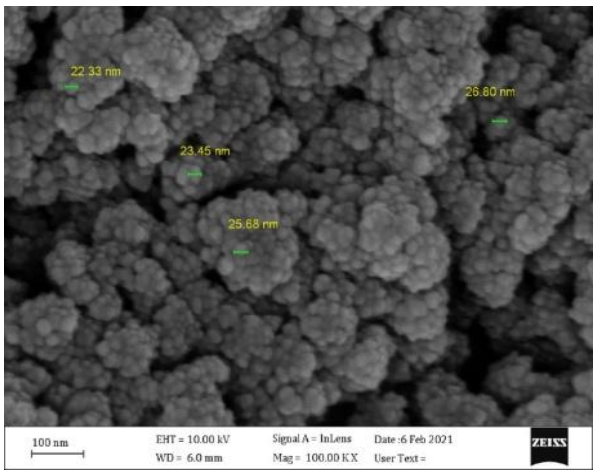

(a) Before PC degradation

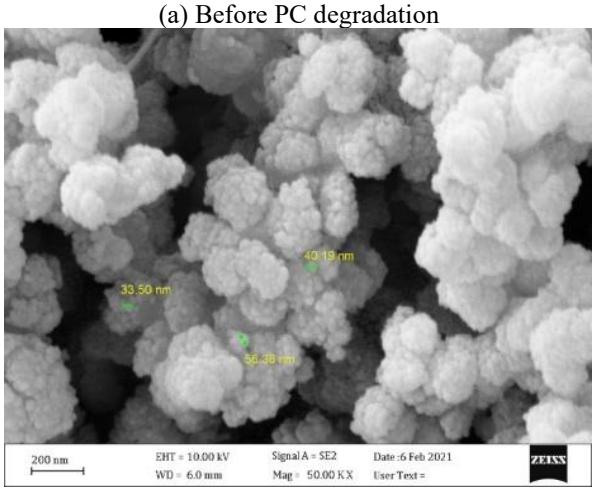

(b) After PC degradation

Figure 5. Scanning Electron Microscopy (SEM) analysis for E-TiO_2

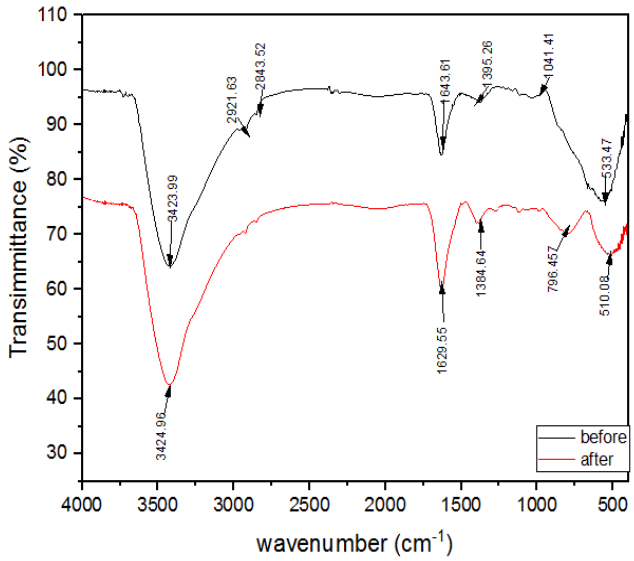

Figure 6. Fourier Transform Infrared Spectroscopy (FTIR) analysis for E-TiO_2

3.1.4 Surface area and porosity analysis

The adsorption and desorption isotherms of nitrogen molecules is used to determine the specific surface area and pore size distribution of E-TiO_2 NPs [30]. The synthetic E-TiO_2 NPs have a BET specific surface area of 345.25 m^2/gm. Compared to commercially available chemically produced TiO_2 NPs (< 100 m^2/g), a higher surface area provides a larger number of accessible active sites, enhancing the adsorption of pollutant molecules and facilitating their close contact with photogenerated charge carriers. Consequently, this promotes more efficient photocatalytic degradation by increasing the probability of interfacial redox reactions and reducing mass-

transfer limitations. The enhanced surface area, therefore, plays a critical role in the superior photocatalytic performance observed for the synthesized TiO_2 compared with commercial counterparts. This discussion has been added to the revised manuscript. The results obtained are relatively better [28].

E-TiO_2 nanoparticles have an average pore diameter of 3.7869 nm and a total pore volume of 0.2883 cm^3/gm.

3.2 Photocatalytic activity of E-TiO_2

3.2.1 pH

The impact of pH on the photodegradation process of a solution containing 10 mg/L of PC, 40 mg/L of E-TiO_2, and 250 mg/L of H_2O_2 was investigated in a stir photoreactor at discrete values of pH (3, 5, 7, and 11). The results shown in Figure 7 show that the rate at which the contaminant is degraded is greatly affected by pH during photocatalysis. This figure shows that the maximum elimination of PC is at pH 7, then after that, the rate of degradation increases steadily with the increasing of pH value. It is explained by the fact that this increases the production of hydroxide ions; at high pH levels, more hydroxide ions will be located on the E-TiO_2 surface and can be easily oxidized, increasing the percentage of PC residue elimination [31]. On the other hand, Figure 7 also presents that the removal of PC is lessened at the highest pH levels, and this is mainly due to the intensified surface ionization of E-TiO_2. Here, the study of the point of zero charge (pH_{pzc}) is essential in the process of establishing the pH at which the surface of the catalyst is uncharged overall. That is, the catalyst surface is negatively charged at pH values greater than pH_{pzc} and positively charged at lower pHs [32]. As can be seen by Eqs. (3) and (4), the surface of the photocatalyst can be protonated and deprotonated in the presence of acidic and alkaline conditions, respectively.

$$pH < pH_{pzc} \quad TiOH + H+ \rightarrow TiOH_2{}^+ \tag{3}$$

$$pH > pH_{pzc} \quad TiOH + OH- \rightarrow TiO- + H_2O \tag{4}$$

The point of zero charge (Pzc) of E-TiO_2, which has been extensively studied, was approximately 7.5.

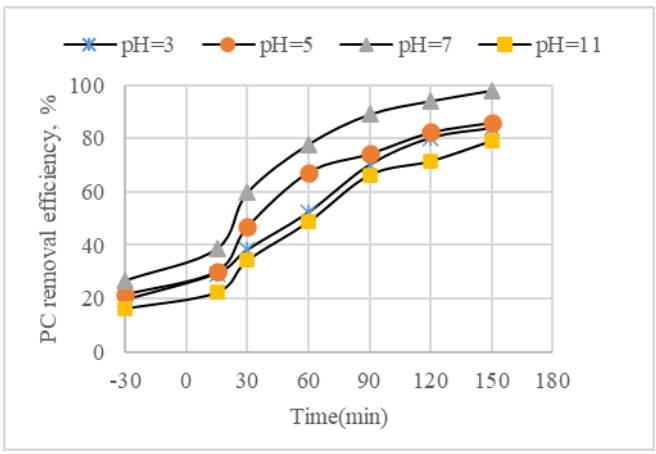

Figure 7. Impact of pH on the PC elimination

In acidic solutions, the E-TiO_2 surface carries a positive charge, whereas in alkaline environments it becomes negatively charged. Electrostatic attraction between paracetamol and E-TiO_2 increases with increasing pH [29], since paracetamol also acquires a negative charge when the pH exceeds 7. Consequently, the degradation efficiency of paracetamol declines at pH values above this level [30].

3.2.2 Initial PC concentration

To assess the impact of PC concentration, the PC loads of 10, 25, and 100 mg/L were tested at constant levels of other variables (pH value of 7, E-TiO_2 of 40 mg/L, and H_2O_2 of 250 mg/L, and 150 min irradiation time). The results are depicted in Figure 8, which demonstrates that the removal efficiency declined as the initial PC concentration increased (94.13, 71, and 57)%, respectively. The two processes explaining the reduction can be the following: First, the rate of free radical generation does not depend on the dose of catalyst, thus when the PC load is increased, the fraction rate of removal is decreased [33]. Second, at high concentrations of PC, additional molecules adsorb onto the catalyst surface, thus blocking active sites and preventing photon propagation to the deeper parts of the nanoparticle [34]. Also, the figure shows that increasing the contact time (120 to 150 minutes) results in a slight increase in degradation with additional increasing contact time, but the results are insignificant, which may be attributed to the limited supply of PC and H_2O_2. These results are in line with the findings of research [35].

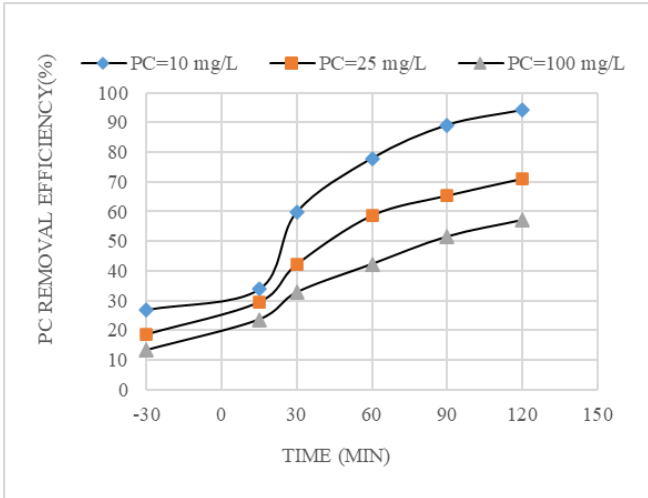

Figure 8. Impact of PC dosage on the photocatalytic system's elimination

3.2.3 H_2O_2 concentration

Figure 9 shows the effects of various concentrations of H_2O_2 (150–600 mg/L) on the degradation rate of 10 mg/L of PC in aqueous solution were examined under constant conditions of E-TiO_2 dosage (40 mg/L), pH (7), and irradiation time (120 min). According to the findings, the degradation efficiency of PC decreased from 94.13% to 58.3% as the H_2O_2 concentration increased from 250 to 600 mg/L. Therefore, the ideal H_2O_2 concentration for photo-oxidation was 250 mg/L. Low H_2O_2 concentrations enhance the rate of photocatalysis, whereas higher concentrations inhibit it. At low H_2O_2 concentrations, photolysis generates hydroxyl radicals, as shown in Eq. (5). Since H_2O_2 is a more effective electron scavenger than O_2, it helps minimize electron–hole recombination. However, at high concentrations, H_2O_2 reacts with E-TiO_2 to generate HO_2• radicals (Eq. (7)), which have a lower oxidative potential than OH• [36].

$$H_2O_2 + hv \rightarrow 2OH^{\cdot} \tag{5}$$

$$H_2O_2 + e- \rightarrow {}^{\cdot}OH + OH^- \quad (6)$$

$$OH + H_2O_2 \rightarrow H_2O + HO_2 \quad (7)$$

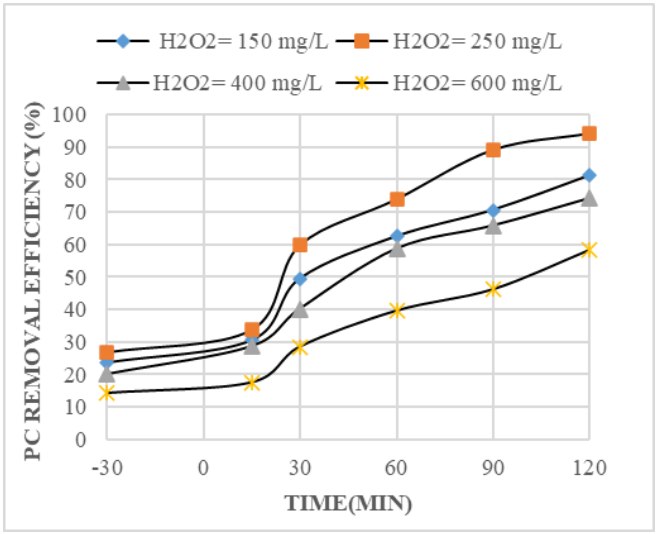

Figure 9. Impact of H_2O_2 dosage on PC degradation by photocatalytic system

3.2.4 Type and concentration of catalyst

The amount of catalyst is also essential for the photocatalytic elimination of PC. Experiments where the E-TiO_2 dose was varied between 20 and 100 mg L^{-1} as shown in Figure 10 shows that the rate of degradation is high at the concentration of 40 mg L^{-1} (94.13%) and decreases with a higher concentration of the catalyst. The light penetration, as opposed to the availability of surface active-sites, can explain this trend in that as the catalyst load increases, so does the total active surface area, but the nanoparticles aggregation increases, and the light scattering, thereby reducing the effective irradiation of the suspension [37]. All these observations are in agreement with the activation steps of E-TiO_2 to the sun radiation [38].

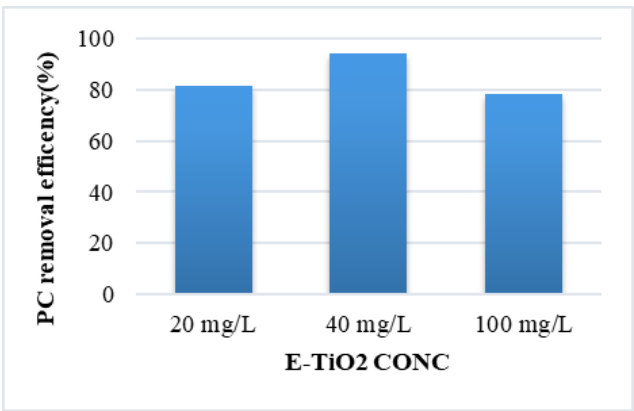

Figure 10. Impact of E-TiO_2 concentration on PC elimination

$$\text{E-}TiO_2 + hv \rightarrow e^- + h^+ \quad (8)$$

$$e^- + O_2 \rightarrow O_2{}^{\cdot -} \quad (9)$$

where, h^+ and e^- are potent agents of oxidation and reduction, respectively. The following is an expression for the oxidative and reductive reaction steps:

- Oxidative reaction:

$$h^+ + organic \rightarrow CO_2 \quad (10)$$

$$h^+ + H_2O \rightarrow {}^{\cdot}OH + H \quad (11)$$

- Reductive reaction:

$$OH + organic \rightarrow CO_2 \quad (12)$$

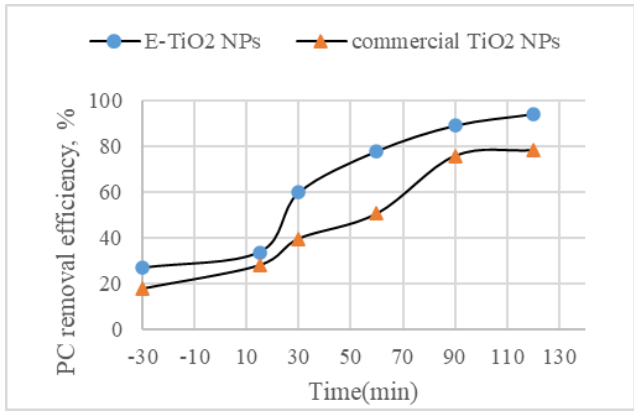

Figure 11. Influence of TiO_2-type catalyst on PC degradation

To determine the efficiency of E-TiO_2 synthesis, an experiment was conducted using commercial TiO_2 under optimal operating conditions. The percentage elimination of the PC drug residue is higher when E-TiO_2 is used than when commercial TiO_2 is used; at 40 mg/L of E-TiO_2 and TiO_2, the removal efficiency showed an increment ratio of more than 19.8%, as indicated in Figure 11.

3.3. Recyclability of E-TiO_2 NPs

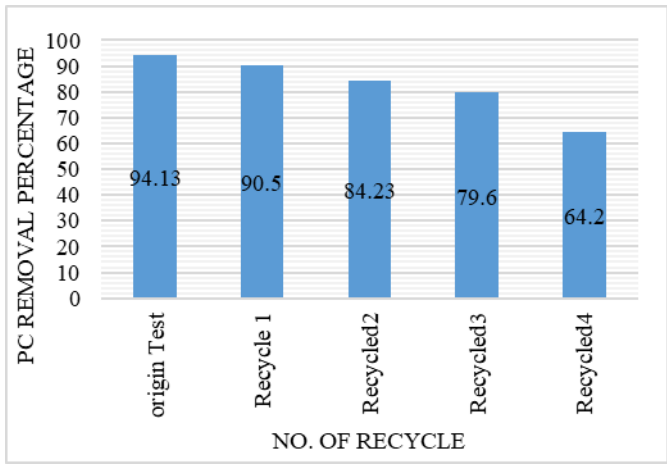

Figure 12. The reusability of E-TiO_2 nanoparticles for the degradation of PC

A 180-minute experimental series was performed at a pH value of 7 using 40 mg/L of E-TiO_2, 10 mg/L of paracetamol, and 250 mg/L of H_2O_2 to evaluate the performance of the reused photocatalyst. The corresponding results are presented in Figure 12. Across five uses conducted over four successive recycling cycles, the catalyst achieved efficiencies of 94.13%, 90.5%, 84.23%, 79.6%, and 64.2%, respectively. The gradual decline in degradation efficiency can be linked to the partial catalyst loss during filtration [39]. With repeated reuse,

previously active surface regions become unavailable for paracetamol adsorption and photon absorption, thereby diminishing photocatalytic activity [40]. Overall, the observed performance confirms the reusability of the E-TiO_2 nanoparticles.

3.4 Total organic carbon

The complete decomposition of organic materials to H_2O and CO_2 is known as mineralization. Therefore, the goal of any photocatalytic process should be to achieve a thorough mineralization. Monitoring the treated samples' total organic carbon (TOC) readings can reveal the extent of mineralization. TOC is considered the most relevant for the determination of organic pollution [41]. The TOC values of PC after photocatalytic treatment with E-TiO_2 samples are given in Figure 13. It is clearly shown that a reduction in the concentration of TOC occurs as a function of time. Also, this figure shows that the use of hydrogen peroxide increases the total organic carbon decomposition by providing a greater number of hydroxyl radicals [42]. TOC is thought to be the most significant variable in determining organic contamination.

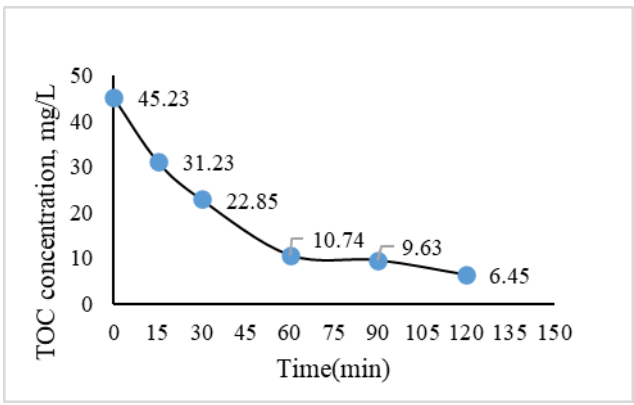

Figure 13. The mineralization process of PC using E-TiO_2 NPs

3.5 Photo degradation kinetics

Understanding the photodegradation process and reaction rate, which rely on the dynamic interaction of PC and the nanocomposite surface, requires kinetic modelling. The pseudo-first-order kinetics model (Eq. (13)) was used in this study.

$$\ln\frac{C}{C_o} = K_{obs}.t \qquad (13)$$

where, K_{obs} (1/min) represents the reaction rate constant for pseudo-first-order, C_o and C (mg/L) are the initial and final concentrations of PC at irradiation time t, respectively (min). The kinetics results are obtained by plotting $\ln\frac{C}{C_o}$ as a function of t ranging between 0 and 150 min, as seen in Figure 14, and tabulated in Table 2.

The outcome demonstrates that increasing the concentration of PC at the beginning reduces the constant of degradation rate (K_{obs}) and higher R^2 values (more than 98%), which demonstrates the photodegradation over E-TiO_2, followed by this model, which was consistent with the investigational findings cited in section 3.2.2.

Table 2. The parameters of the reaction rate for PC elimination in the photocatalyst

PC Dosage (mg/L)	Percentage of Removal % at 150 min	First-Order	
		R^2	K_{obs} (min^{-1})
10	98.03	0.9833	0.0244
25	86.23	0.9955	0.0118
50	65.32	0993	0.0057
100	54	0.9955	0.0044

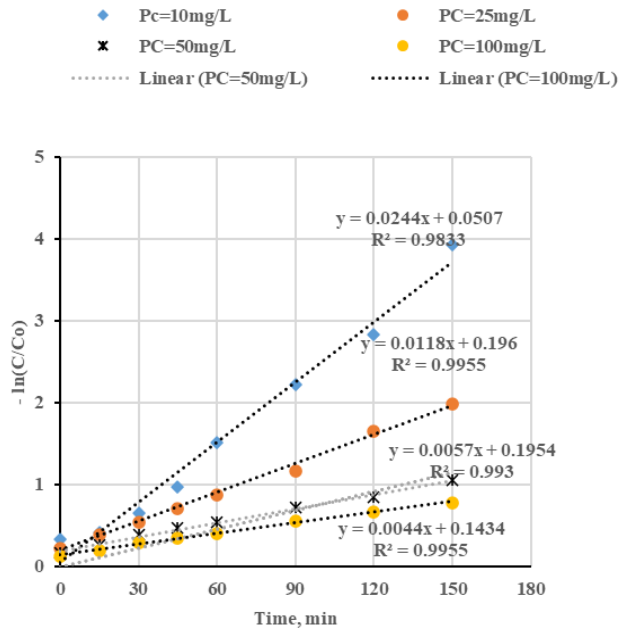

Figure 14. pseudo-first-order kinetics model for PC degradation at various beginning concentrations

4. CONCLUSION

In this research, titanium oxide nanoparticles were successfully prepared using *Eucalyptus globulus* leaves (denoted as E-TiO_2) extract, characterized, and then used to remove PC residual in aqueous solution by using a batch mode reactor. Characteristic analysis proved the heterogeneous texture, rough surface, and absence of any secondary phases or impurity peaks. The efficacy of E- TiO_2 was measured in a batch reactor under the sunlight with the following parameters (pH, PC concentration, time of irradiation, concentration of E-TiO_2, and H_2O_2). And the maximum removal efficiency reached 94.13% at an optimum condition of pH 7, PC 10 mg/L, E-TiO_2 of 40 mg/L, and H_2O_2 of 250 mg/L, and irradiation time of 120 min, while only 78.23% of PC was removed by using commercial TiO_2 at the same operation conditions. The findings also show that the rate constant of the pseudo-first order model for first-order degradation is decreased with increasing the initial PC concentration, and the high values of R^2 of the degradation curves under different PC loads prove that the photodegradation follows a pseudo-first order model. As a result, this cheap catalyst has a significant photocatalytic activity, which makes it possible to consider it a green photocatalyst that is able to remove the pollutant under sunlight.

ACKNOWLEDGMENT

The authors are grateful for the financial and scientific support from the University of Baghdad.

REFERENCES

[1] Klavarioti, M., Mantzavinos, D., Kassinos, D. (2009). Removal of residual pharmaceuticals from aqueous systems by advanced oxidation processes. Environment International, 35(2): 402-417. https://doi.org/10.1016/j.envint.2008.07.009

[2] Xu, Y., Yang, X., Liang, C., Peng, L. (2025). Efficient adsorption and photocatalytic degradation of pharmaceutical compounds by Bi24O31Br10: Mechanism, toxicity assessment, and degradation pathways. Journal of Water Process Engineering, 71: 107233. https://doi.org/10.1016/j.jwpe.2025.107233

[3] Chau, J.H.F., Lai, C.W., Leo, B.F., Juan, J.C., Johan, M.R. (2022). Advanced photocatalytic degradation of acetaminophen using $Cu_2O/WO_3/TiO_2$ ternary composite under solar irradiation. Catalysis Communications, 163: 106396. https://doi.org/10.1016/j.catcom.2022.106396

[4] Ali, A.H., Alwared, A.I. (2025). Solar-photocatalytic degradation of paracetamol using Zeolite/Fe_3O_4/CuS/$CuWO_4$ pn heterojunction: Synthesis, characterization and its application. Solar Energy, 290: 113383. https://doi.org/10.1016/j.solener.2025.113383

[5] Manu, B., Mahamood, S., Vittal, H., Shrihari, S. (2011). A novel catalytic route to degrade paracetamol by Fenton process. International Journal of Research in Chemistry and Environment, 1(1): 157-164.

[6] Mohammed, N.A., Alwared, A.I., Salman, M.S. (2020). Photocatalytic degradation of reactive yellow dye in wastewater using H_2O_2/TiO_2/UV technique. Iraqi Journal of Chemical and Petroleum Engineering, 21(1): 15-21. https://doi.org/10.31699/IJCPE.2020.1.3

[7] Nashmi, O.A., Mohammed, A.A., Abdulrazzaq, N.N. (2020). Investigation of ozone microbubbles for the degradation of methylene orange contaminated wastewater. Iraqi Journal of Chemical and Petroleum Engineering, 21(2): 25-35. https://doi.org/10.31699/IJCPE.2020.2.4

[8] Mohammed, A.A., Hammood, Z.A. (2025). Efficient removal of sulfamethoxazole antibiotic from aqueous solution using red mud/layered double hydroxide nanocomposite: Optimization, kinetic, and isotherm studies. Results in Surfaces and Interfaces, 19: 100534. https://doi.org/10.1016/j.rsurfi.2025.100534

[9] Al-Anssari, S., Hassan, H.A., Mohsin, M.K., Mohammed, A.A. (2025). Influence of zinc oxide nanoparticles on the efficiency of oxytetracycline removal from wastewater using continuous catalytic ozonation. International Journal of Nanoelectronics and Materials, 18: 175-187. https://doi.org/10.58915/ijneam.v18iJune.2341

[10] Ismail, G.A., Sakai, H. (2022). Review on effect of different type of dyes on advanced oxidation processes (AOPs) for textile color removal. Chemosphere, 291: 132906. https://doi.org/10.1016/j.chemosphere.2021.132906

[11] Mustafa, Y.A., Alwared, A.I., Ebrahim, M. (2014). Heterogeneous photocatalytic degradation for treatment of oil from wastewater. Al-Khwarizmi Engineering Journal, 10(3): 53-61.

[12] Balaji, S., Guda, R., Mandal, B.K., Kasula, M., Ubba, E., Khan, F.R.N. (2021). Green synthesis of nano-titania (TiO_2 NPs) utilizing aqueous Eucalyptus globulus leaf extract: Applications in the synthesis of 4 H-pyran derivatives. Research on Chemical Intermediates, 47(9): 3919-3931. https://doi.org/10.1007/s11164-018-03720-0

[13] Salgado, P., Mártire, D.O., Vidal, G. (2019). Eucalyptus extracts-mediated synthesis of metallic and metal oxide nanoparticles: Current status and perspectives. Materials Research Express, 6(8): 082006. https://doi.org/10.1088/2053-1591/ab254c

[14] Alobaidi, T.B., Alwared, A.I. (2022). Biosynthetic of titanium dioxide nanoparticles using Zizyphus spina-christi leaves extract. Journal of Ecological Engineering, 23(1): 315-324. https://doi.org/10.12911/22998993/143971

[15] Pushpamalini, T., Keerthana, M., Sangavi, R., Nagaraj, A., Kamaraj, P. (2021). Comparative analysis of green synthesis of TiO_2 nanoparticles using four different leaf extract. Materials Today: Proceedings, 40(S1): S180-S184. https://doi.org/10.1016/j.matpr.2020.08.438

[16] Abdulrazaq, H.A., Alwared, A.I. (2024). Bio-synthesis of TiO_2 using grape leaves extract and its application for photocatalytic degradation of ibuprofen from aqueous solution. Environmental Technology, 45(13): 2493-2505. https://doi.org/10.1080/09593330.2023.2176791

[17] Patidar, V., Jain, P. (2017). Green synthesis of TiO_2 nanoparticle using Moringa oleifera leaf extract. International Research Journal of Engineering and Technology, 4(3): 470-473.

[18] Ali, G.A., Habeeb, O.A., Algarni, H., Chong, K.F. (2019). CaO impregnated highly porous honeycomb activated carbon from agriculture waste: symmetrical supercapacitor study. Journal of Materials Science, 54(1): 683-692. https://doi.org/10.1007/s10853-018-2871-6

[19] Vijayaraghavan, K., Ashokkumar, T. (2017). Plant-mediated biosynthesis of metallic nanoparticles: A review of literature, factors affecting synthesis, characterization techniques and applications. Journal of Environmental Chemical Engineering, 5(5): 4866-4883. https://doi.org/10.1016/j.jece.2017.09.026

[20] Wang, X., Wang, A., Ma, J., Fu, M. (2017). Facile green synthesis of functional nanoscale zero-valent iron and studies of its activity toward ultrasound-enhanced decolorization of cationic dyes. Chemosphere, 166: 80-88. https://doi.org/10.1016/j.chemosphere.2016.09.056

[21] Torres-Limiñana, J., Feregrino-Pérez, A.A., Vega-González, M., Escobar-Alarcón, L., Cervantes-Chávez, J.A., Esquivel, K. (2022). Green synthesis via eucalyptus globulus l. extract of Ag-TiO_2 catalyst: Antimicrobial activity evaluation toward water disinfection process. Nanomaterials, 12(11): 1944. https://doi.org/10.3390/nano12111944

[22] Uwaya, G.E., Naidoo, L., Bisetty, K. (2023). Novel characterization of the interaction between EVF drug and TiO_2. Surfaces and Interfaces, 40: 103057. https://doi.org/10.1016/j.surfin.2023.103057

[23] Oscier, C.D., Milner, Q.J.W. (2009). Peri-operative use of paracetamol. Anaesthesia, 64(1): 65-72. https://doi.org/10.1111/j.1365-2044.2008.05674.x

[24] Spaltro, A., Pila, M.N., Colasurdo, D.D., Grau, E.N., Román, G., Simonetti, S., Ruiz, D.L. (2021). Removal of

paracetamol from aqueous solution by activated carbon and silica. Experimental and computational study. Journal of Contaminant Hydrology, 236: 103739. https://doi.org/10.1016/j.jconhyd.2020.103739

[25] Huang, J., Li, Q., Sun, D., Lu, Y., Su, Y., Yang, X., Chen, C. (2007). Biosynthesis of silver and gold nanoparticles by novel sundried Cinnamomum camphora leaf. Nanotechnology, 18(10): 105104. https://doi.org/10.1088/0957-4484/18/10/105104

[26] Chatterjee, A., Nishanthini, D., Sandhiya, N., Abraham, J. (2016). Biosynthesis of titanium dioxide nanoparticles using Vigna radiata. Asian Journal of Pharmaceutical and Clinical Research, 9(4): 85-88.

[27] Malakootian, M., Nasiri, A., Amiri Gharaghani, M. (2020). Photocatalytic degradation of ciprofloxacin antibiotic by TiO_2 nanoparticles immobilized on a glass plate. Chemical Engineering Communications, 207(1): 56-72. https://doi.org/10.1080/00986445.2019.1573168

[28] Mohammed, A.A., Al-Musawi, T.J., Kareem, S.L., Zarrabi, M., Al-Ma'abreh, A.M. (2020). Simultaneous adsorption of tetracycline, amoxicillin, and ciprofloxacin by pistachio shell powder coated with zinc oxide nanoparticles. Arabian Journal of Chemistry, 13(3): 4629-4643. https://doi.org/10.1016/j.arabjc.2019.10.010

[29] Sulaiman, F.A., Alwared, A.I. (2022). Green synthesis of TiO_2 using Ocimum basilicum leaf extract and its application in photocatalytic degradation of amoxicillin residues from aqueous solution. Desalination and Water Treatment, 262: 312-322. https://doi.org/10.5004/dwt.2022.28504

[30] Du, J., Sun, H. (2014). Polymer/TiO_2 hybrid vesicles for excellent UV screening and effective encapsulation of antioxidant agents. ACS Applied Materials & Interfaces, 6(16): 13535-13541. https://doi.org/10.1021/am502663j

[31] Borges, M.E., García, D.M., Hernández, T., Ruiz-Morales, J.C., Esparza, P. (2015). Supported photocatalyst for removal of emerging contaminants from wastewater in a continuous packed-bed photoreactor configuration. Catalysts, 5(1): 77-87. https://doi.org/10.3390/catal5010077

[32] Sun, Y., Yue, Q., Gao, B., Wang, B., Li, Q., Huang, L., Xu, X. (2012). Comparison of activated carbons from *Arundo donax Linn* with $H_4P_2O_7$ activation by conventional and microwave heating methods. Chemical Engineering Journal, 192: 308-314. https://doi.org/10.1016/j.cej.2012.04.007

[33] Khodadadi, M., Ehrampoush, M.H., Ghaneian, M.T., Allahresani, A., Mahvi, A.H. (2018). Synthesis and characterizations of $FeNi_3$@SiO_2@TiO_2 nanocomposite and its application in photo-catalytic degradation of tetracycline in simulated wastewater. Journal of Molecular Liquids, 255: 224-232. https://doi.org/10.1016/j.molliq.2017.11.137

[34] Oskoei, V., Dehghani, M.H., Nazmara, S., Heibati, B., Asif, M., Tyagi, I., Gupta, V.K. (2016). Removal of humic acid from aqueous solution using UV/ZnO nano-photocatalysis and adsorption. Journal of Molecular Liquids, 213: 374-380. https://doi.org/10.1016/j.molliq.2015.07.052.

[35] Turkay, G.K., Kumbur, H. (2019). Investigation of amoxicillin removal from aqueous solution by Fenton and photocatalytic oxidation processes. Kuwait Journal of Science, 46(2): 85-93.

[36] Qin, C., Yang, S., Sun, C., Zhan, M., Wang, R., Cai, H., Zhou, J. (2010). Investigation of the effects of humic acid and H_2O_2 on the photocatalytic degradation of atrazine assisted by microwave. Frontiers of Environmental Science & Engineering in China, 4(3): 321-328. https://doi.org/10.1007/s11783-010-0238-6

[37] Mohammadi, R., Massoumi, B., Rabani, M. (2012). Photocatalytic decomposition of amoxicillin trihydrate antibiotic in aqueous solutions under UV irradiation using Sn/TiO_2 nanoparticles. International Journal of Photoenergy, 2012(1): 514856. https://doi.org/10.1155/2012/514856

[38] Ahmed, S., Rasul, M.G., Martens, W.N., Brown, R., Hashib, M.A. (2010). Heterogeneous photocatalytic degradation of phenols in wastewater: A review on current status and developments. Desalination, 261(1-2): 3-18. https://doi.org/10.1016/j.desal.2010.04.062

[39] Moosavi, S., Li, R.Y.M., Lai, C.W., Yusof, Y., Gan, S., Akbarzadeh, O., Johan, M.R. (2020). Methylene blue dye photocatalytic degradation over synthesised Fe_3O_4/AC/TiO_2 nano-catalyst: Degradation and reusability studies. Nanomaterials, 10(12): 2360. https://doi.org/10.3390/nano10122360

[40] Al-Musawi, T.J., Mengelizadeh, N., Alwared, A.I., Balarak, D., Sabaghi, R. (2023). Photocatalytic degradation of ciprofloxacin by MMT/$CuFe_2O_4$ nanocomposite: Characteristics, response surface methodology, and toxicity analyses. Environmental Science and Pollution Research, 30(27): 70076-70093. https://doi.org/10.1007/s11356-023-27277-7

[41] Nawawi, W.I., Nawi, M.A. (2014). Carbon coated nitrogen doped P25 for the photocatalytic removal of organic pollutants under solar and low energy visible light irradiations. Journal of Molecular Catalysis A: Chemical, 383-384: 83-93. https://doi.org/10.1016/j.molcata.2013.11.030

[42] Loaiza-Ambuludi, S., Panizza, M., Oturan, N., Oturan, M.A. (2014). Removal of the anti-inflammatory drug ibuprofen from water using homogeneous photocatalysis. Catalysis Today, 224: 29-33. https://doi.org/10.1016/j.cattod.2013.12.018